In Vivo Infrared Tomographic Imaging of Laser-Heated Blood Vessels

Sergey A. Telenkov, B. Samuel Tanenbaum, *Senior Member, IEEE,*
Dennis M. Goodman, J. Stuart Nelson, and Thomas E. Milner

***Abstract*—We demonstrate a method for infrared tomographic imaging of the initial three-dimensional (3-D) temperature increase of *in vivo* blood vessels following pulsed laser exposure. Using a time-sequence of infrared images recorded by a fast focal plane array camera as input data, a reconstruction algorithm is used to compute the initial 3-D temperature increases in the chick chorioallantoic membrane and port wine stain in human skin. The noncontact tomographic imaging method is relevant to various laser therapies that rely on a photothermal mechanism for selective modification of tissue and may find diagnostic application to determine optimal laser dosimetry, position, and size of targeted subsurface chromophores.**

***Index Terms*—Focal plane array, imaging, infrared, port wine stain, tomography.**

I. Introduction

INFRARED (IR) imaging of biological materials provides a noncontact technique to determine the temperature increase in tissues following pulsed laser exposure. Selective absorption of laser radiation in subsurface chromophores results in localized heating and may be detected as an increase in IR emission at the air-tissue interface. Pulsed photothermal radiometry has been utilized in numerous studies to determine optical and thermal properties of opaque materials [1], [2] as well as nondestructive inspection of composite structures [3]. Theoretical analysis of photothermal phenomena in a one-dimensional (1-D) model was given in early work by Leung and Tam [4]. Their analysis demonstrated that the IR signal recorded immediately following pulsed laser exposure may be used to determine the thermal diffusivity and optical absorption coefficient at the excitation wavelength of a light-absorbing sample.

Increasing use of laser sources for treatment of skin vascular disorders such as port wine stain (PWS) [5], skin resurfacing [6], and tissue reshaping [7] has stimulated theoretical and experimental research on photothermal effects in tissue in response to pulsed laser exposure. Inasmuch as blood hemoglobin is an important skin chromophore in the 570–590-nm spectral band, use of pulsed laser radiation is a convenient modality for selective photothermal damage of blood vessels comprising vascular lesions. Duration of pulsed irradiation and peak temperature increase produced in the targeted blood vessels are crucial parameters for successful laser therapy [8].

In contrast to alternative diagnostic imaging techniques that rely principally on the detection of remitted or frequency converted light from the irradiated tissue (e.g., optical coherence tomography [9], photon diffusion [10], ultrasonic modulation of diffusing light [11], spectral imaging reflectometry [12], and two-photon fluorescence [13]), photoacoustic and photothermal imaging techniques provide a signal amplitude that is directly related to the initial space-dependent temperature increase in targeted chromophores resulting from absorption of pulsed radiation. Although the photoacoustic technique is potentially advantageous for imaging deep chromophores, reported applications require mechanical contact between the sensor and tissue as well as use of a scanning algorithm for data acquisition and image reconstruction [14]. The photothermal imaging technique we describe takes advantage of a variety of commercially available IR detector arrays to collect the signal remotely from an extended object after pulsed laser exposure. A mathematical model and tomographic reconstruction algorithm (TRA) may be applied to process IR images and compute the initial three-dimensional (3-D) temperature increase in tissue. The computed temperature increase in a target object provides data for analysis of position and size of subsurface blood vessels and peak temperatures induced by absorption of pulsed laser radiation. This information is important for a variety of biomedical applications involving laser-tissue interaction including treatment of PWS.

We describe application of an IR imaging technique for *in vivo* 3-D tomographic reconstruction of laser-heated blood vessels. An iterative nonnegatively constrained conjugate gradient reconstruction algorithm was developed to compute the initial 3-D temperature distribution from a time-sequence of IR images recorded by a high-speed focal plane array (FPA) camera. First, we applied this technique to reconstruct the laser-induced temperature increase in the vasculature of the chick chorioallantoic membrane (CAM). Second, application of the method is demonstrated to compute the initial 3-D temperature increase in PWS blood vessels immediately following pulsed laser exposure.

Manuscript received January 4, 1999; revised April 12, 1999. This work was supported by The Whitaker Foundation under Biomedical Investigator Award WF-21025 and by the Institutes of Arthritis, Musculoskeletal, and Skin Disease under Grant AR-43419 and by the Heart Lung and Blood Institute at the National Institutes of Health.

S. A. Telenkov and T. E. Milner are with the Biomedical Engineering Program, University of Texas at Austin, Austin, TX 78712 USA.

B. S. Tanenbaum is with the Department of Engineering, Harvey Mudd College, Claremont, CA 91711 USA.

D. M. Goodman is with Lawrence Livermore National Laboratory, University of California, Livermore, CA 94550 USA.

J. S. Nelson is with the Beckman Laser Institute and Medical Clinic, University of California, Irvine, CA 92612 USA.

Publisher Item Identifier S 1077-260X(99)07510-3.

II. Background and Theory

For the purpose of analysis, we model subsurface blood vessels as a distribution of discrete light-absorbing chromophores. To characterize the thermal response of tissue to pulsed laser exposure we use the 3-D bio-heat equation to determine the space-time temperature increase $\Delta T(x,y,z,t)$ [15]:

$$\nabla^2(\Delta T) - \frac{1}{\chi}\frac{\partial(\Delta T)}{\partial t} - \frac{Q}{\chi}(\Delta T) = 0 \tag{1}$$

with a Robin-type boundary condition at the air–skin interface:

$$\kappa \left.\frac{\partial \Delta T}{\partial z}\right|_{z=0} - h\Delta T|_{z=0} = 0 \tag{2}$$

where Q is the rate of blood perfusion, κ and χ denote the heat conduction coefficient and thermal diffusivity of human skin respectively, which we assume is homogeneous, h represents the combined radiative and convective heat loss at the air–skin interface. The Green's function solution to (1)–(2) represents temperature increase in skin at position (x,y,z) and time (t) in response to instantaneous release of a point heat source at the $(0,0,\zeta_0)$ and time $t=0$:

$$G(x,y,z,t;\zeta_0) = \frac{e^{-Qt}}{(4\pi\chi t)^{3/2}} e^{-(x^2+y^2)/4\chi t}\left\{e^{-(z-\zeta_0)^2/4\chi t} + e^{-(z+\zeta_0)^2/4\chi t} \cdot \left[1 - \frac{h}{k}\sqrt{4\pi\chi t}\cdot \mathrm{erfcx}(u)\right]\right\} \tag{3}$$

where

$$u = \frac{z+\zeta_0}{2\sqrt{\chi t}} + \frac{h}{\kappa}\sqrt{\chi t}$$

and $\mathrm{erfcx}(u) = \exp(u)^2\mathrm{erfc}(u)$, where $\mathrm{erfc}(\cdot)$ is the complimentary error function.

Because the FPA camera records IR emission at the air–skin interface, we describe the radiometric temperature increase by the thermal point spread function (K_T) obtained by summing the contributions of infrared emission at all depths (z) in the tissue

$$K_T(x,y,t;\zeta_0) = \int_{z=0}^{z=\infty} \mu_{\mathrm{ir}} e^{-\mu_{\mathrm{ir}} z}\cdot G(x,y,z,t;\zeta_0)\cdot dz \tag{4}$$

where μ_{ir} is the infrared attenuation coefficient of tissue which we assume is homogeneous. Substitution of the Green's function (3) into (4) gives an analytic expression for the thermal point spread function K_T

$$K_T(x,y,t;\zeta_0) = \frac{e^{-Qt}}{4\pi\chi t} e^{-(x^2+y^2)/4\chi t}\cdot\frac{\mu_{\mathrm{ir}}}{2}{}^{-\zeta_0^2/4\chi t} \cdot\left\{\mathrm{erfcx}(u_+) + \mathrm{erfcx}(u_-) - \frac{2(h/\kappa)}{(h/\kappa)-\mu_{\mathrm{ir}}}[\mathrm{erfcx}(u_+) - \mathrm{erfcx}(u_1)]\right\} \tag{5}$$

where

$$u_\pm = \mu_{\mathrm{ir}}\sqrt{\chi t} \pm \frac{\zeta_0}{2\sqrt{\chi t}}, \quad u_1 = \frac{h}{\kappa}\sqrt{\chi t} + \frac{\zeta_0}{2\sqrt{\chi t}}.$$

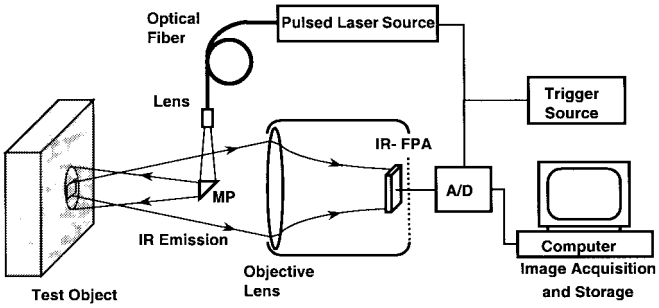

Fig. 1. Experimental apparatus for IR imaging of laser-heated blood vessels. MP: Microprism. IR-FPA: Infrared focal plane array. A/D: analog-to-digital converter.

Because the relaxation time due to blood perfusion $(1/Q)$ in the microvasculature is much longer than the time of measurement, i.e., $t \ll 1/Q$, (5) may be written as the product of two terms K_r and K_z that represent heat diffusion parallel and perpendicular to the air–skin interface, respectively

$$K_T(x-\xi, y-\eta, t;\zeta_0) = K_r(x-\xi, y-\eta, t)\cdot K_z(t,\zeta_0) \tag{6}$$

where,

$$K_r(x,y,t) = \frac{1}{4\pi\chi t} e^{-(x^2+y^2)/4\pi\chi t}, \tag{7}$$

$$K_z(t,\zeta_0) = \frac{\mu_{\mathrm{ir}}}{2} e^{-\zeta_0^2/4\chi t}\left\{\mathrm{erfcx}(u_+) + \mathrm{erfcx}(u_-) - \frac{2h/\kappa}{h/\kappa - \mu_{\mathrm{ir}}}[\mathrm{erfcx}(u_+) - \mathrm{erfcx}(u_1)]\right\}. \tag{8}$$

Using (6)–(8), we may write an expression for the radiometric temperature increase $\Delta R(x,y,t)$ at the air–skin interface due to the initial laser-induced temperature distribution $\Delta T(x,y,z,t=0)$ as a convolution integral

$$\Delta R(x,y,t) = \iint_{\xi,\eta} K_r(x-\xi, y-\eta, t)\, d\xi\, d\eta \cdot\left[\int_\zeta K_z(t,\zeta)\cdot\Delta T(\xi,\eta,\zeta,t=0)\, d\zeta\right] = K_r * \left[\int_\zeta K_z(t,\zeta)\cdot\Delta T(\xi,\eta,\zeta,t=0)\, d\zeta\right] \tag{9}$$

where symbol $(*)$ denotes a convolution operator. Immediately following pulsed laser exposure, infrared emission from subsurface chromophores positioned near the surface $(\zeta \approx 1/\mu_{\mathrm{ir}})$ transmits directly through the air–skin interface and into the objective lens of the IR-FPA camera giving a peak response of the radiometric temperature increase. Alternatively, infrared emission from deep chromophores $(\zeta \gg 1/\mu_{\mathrm{ir}})$ is strongly attenuated and radiometric temperature increase due to heat diffusion to the surface is dominant resulting in a blurred IR image at a later time $t \approx \zeta^2/4\chi$.

Limited spatial resolution of the IR-FPA camera introduces additional blur into recorded IR images. To account for such limitations of the imaging instrumentation, we compute the camera point spread function K_C and include it into the analysis to obtain an expression relating a sequence of recorded

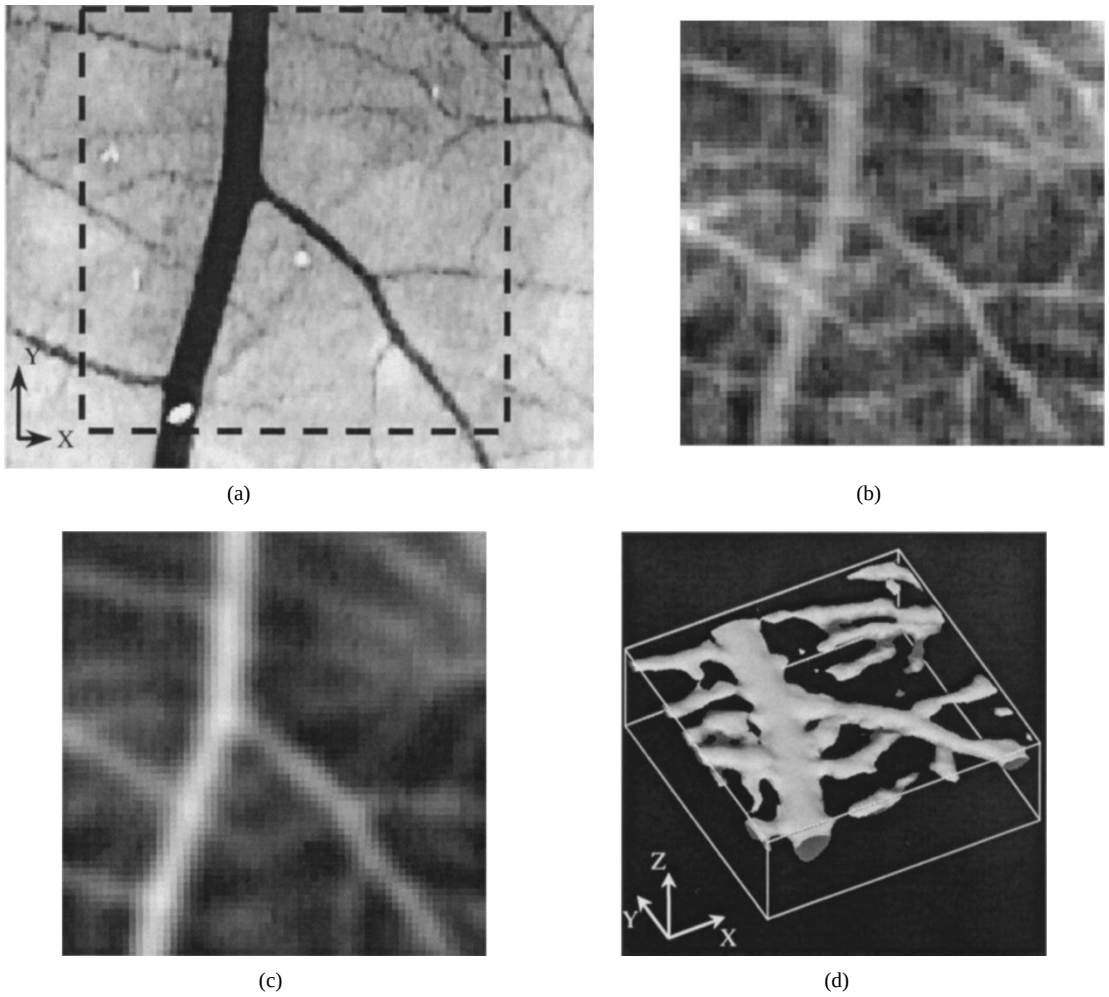

(a) (b)

(c) (d)

Fig. 2. (a) Optical image of the CAM vasculature (imaging area is shown by a dashed line). Photothermal responses of the CAM (b) immediately and (c) 8 ms following pulsed laser exposure at 3.4 J/cm^2 and $t_p = 5$ ms. (d) Initial 3-D temperature increase computed after 30 iterations of TRA (isothermal surface at $\Delta T = 24\,^{\circ}$C).

infrared emission images $\Delta M(x,y,t)$ to the space-dependent temperature increase $\Delta T(x,y,z,t=0)$ in subsurface blood vessels immediately following pulsed laser exposure

$$\begin{aligned}\Delta M(x,y,t) &= \int_{x',y'} K_C(x-x',y-y')\,dx'\,dy' \\ &\quad \times \iiint_{\xi,\eta,\zeta} K_T(x'-\xi,y'-\eta,\zeta,t) \\ &\quad \cdot \Delta T(\xi,\eta,\zeta;t=0)\cdot d\xi\,d\eta\,d\zeta \\ &= K_C * \Delta R = K_C * K_T * \Delta T. \end{aligned} \tag{10}$$

We utilize imaging equation (10) to compute the initial 3-D temperature increase following pulsed laser exposure from a recorded time-sequence of IR images using an iterative nonnegatively constrained conjugate gradient algorithm. Imposing a nonnegativity constraint on the solution $(\Delta T \geq 0)$ substantially increases the quality of the reconstructed image [16]. Mathematically, determination of $\Delta T(x,y,z,t=0)$ from the recorded time sequence of images constitutes an ill-posed inverse problem which may be written as linear matrix equation:

$$\Delta\mathbf{M} = \mathbf{K_C}\mathbf{K_T}\Delta\mathbf{T} = \mathbf{K}\Delta\mathbf{T} \tag{11}$$

where boldface characters represent discrete vector and matrix quantities. The ill-posed nature of the imaging problem (11) is due to the relatively large number of small singular values of the kernel function $\mathbf{K}$. Various inversion methods can be utilized to estimate a solution for the initial temperature increase $\Delta\mathbf{T}$ [17]. The conjugate gradient algorithm consists of iterative minimization of a residual functional $\mathbf{r}(\Delta\mathbf{T},\lambda)$

$$\mathbf{r}(\Delta\mathbf{T},\lambda) = ||\mathbf{K}\Delta\mathbf{T} - \Delta\mathbf{M}||^2 - \lambda||\Delta\mathbf{T}||^2 \tag{12}$$

where λ is a regularization parameter. We applied the nonnegatively constrained conjugate gradient TRA and regularized by early termination. In this approach, λ is fixed to zero and the number of iterations becomes a regularization parameter. A variety of principles and philosophies exist for specifying the optimal number of iterations [18], [19]. Detailed discussion of various regularization techniques is beyond the scope of this paper and will be reported elsewhere.

III. Experiment

Preliminary experiments were conducted on the CAM microvasculature to demonstrate the IR imaging technique and tomographic reconstruction algorithm in a simple biological

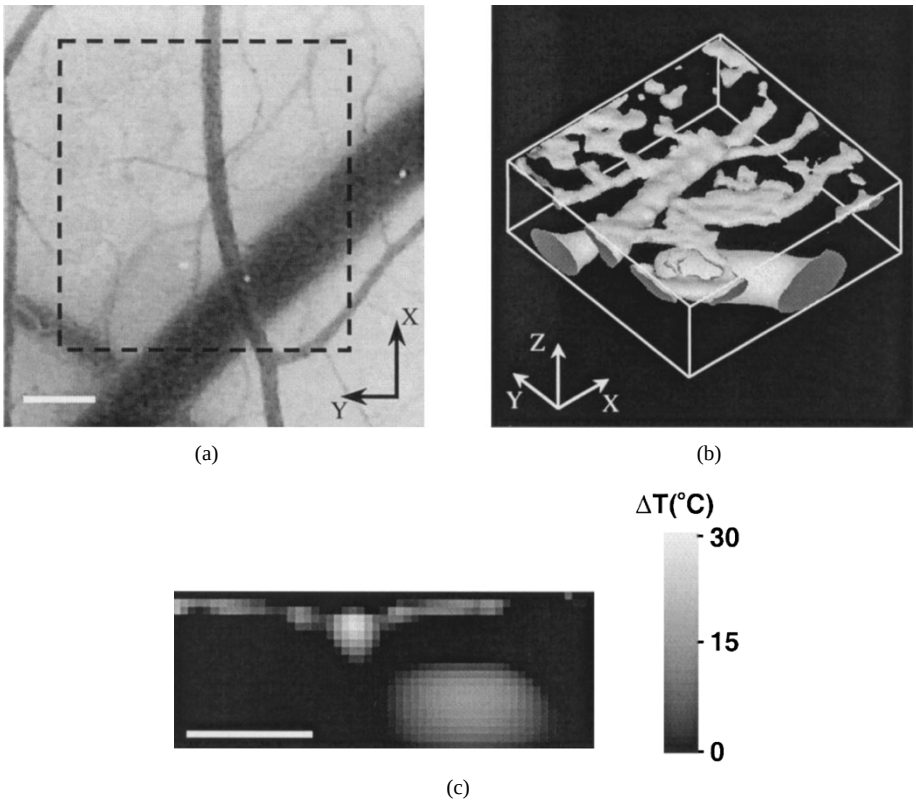

(a) (b)

(c)

Fig. 3. (a) Optical image of the CAM with blood vessels with different calibers. (b) Computed 3-D temperature increase (isothermal surface at 10.5 °C) in CAM blood vessels immediately following pulsed laser exposure at 2.4 J/cm^2 (box dimensions $1.65 \times 1.65 \times 0.6$ mm^3). (c) Cross-sectional image (Y-Z plane) of the computed initial temperature increase. Scale bar equals 500 μm.

model. The experimental setup designed for infrared imaging of laser-heated blood vessels is shown in Fig. 1. Pulsed laser radiation coupled into a 1-mm diameter multimode optical fiber is delivered onto the test object after reflection by a microprism (MP) centered in front of the IR objective lens. Infrared emission from the test object is collected by a unity magnification objective lens ($f/2$, 50 mm diameter) and imaged onto a liquid nitrogen-cooled 256×256 InSb IR-FPA with 30×30 μm^2 pixels (Amber Engineering, Goleta, CA). The infrared signal in the 3–5-μm spectral region is collected by each detector element in the IR-FPA, digitized by a 12-bit A/D converter and stored in the computer's random access memory. The laser and IR-FPA are triggered simultaneously by an external digital delay generator (DG535, Stanford Research Systems, Sunnyvale, CA) and a sequence of four-hundred IR images is acquired for subsequent processing. The digitized signal of each pixel in the time sequence of recorded infrared emission images is independently calibrated for every measurement using a blackbody radiation source. The calibration procedure eliminates inherent nonuniformities in IR images because radiometric temperature is measured using a response curve for each detector in the IR-FPA rather than a single calibration averaged over the entire array.

Each recorded time-sequence of IR emission images was used as input data for our TRA to reconstruct the initial 3-D temperature increase immediately following pulsed laser exposure. The nonnegatively constrained conjugate gradient algorithm was implemented on a Sun Ultra-SPARC Workstation (Sun Microsystems, Mountain View, CA) using C and Fortran 77 programming languages. Numerical solution of the inverse problem is computationally intensive due to the high-dimensional nature of the matrix equation (11). For instance, reconstruction of the initial three-dimensional temperature increase from a sequence of 400 IR images after 40 iterations of the nonnegatively constrained conjugate gradient TRA requires 40–50 min.

IV. Results and Discussion

Because the CAM blood vessels are surrounded by a transparent medium [20] and effects due to light scattering are absent, this biological system allows simultaneous visible and infrared imaging measurements and provides a convenient *in vivo* model to test the IR tomography technique. In our experiments, we used second-harmonic radiation ($\lambda = 532$ nm, $t_p = 2$–10 ms) emitted by a Nd:YAG laser (Coherent, VersaPulse, Santa Clara, CA) to heat CAM blood vessels. The IR-FPA camera was triggered simultaneously with pulsed laser exposure and 400 IR emission images of the CAM recorded at a rate of 1700 frames/s. For high-speed data acquisition, the IR-FPA camera was operated in a 64×64-pixel subregion readout mode, providing a field size of 1.92×1.92 mm^2. Prior to pulsed laser exposure, individual blood vessels were observed under an optical dissection microscope at $40\times$ magnification and recorded by a charge-coupled device (CCD) camera on VHS videotape. The recorded video image of the CAM revealed a dense network of superficial capillaries overlying arteries and veins with larger diameters [Fig. 2(a)].

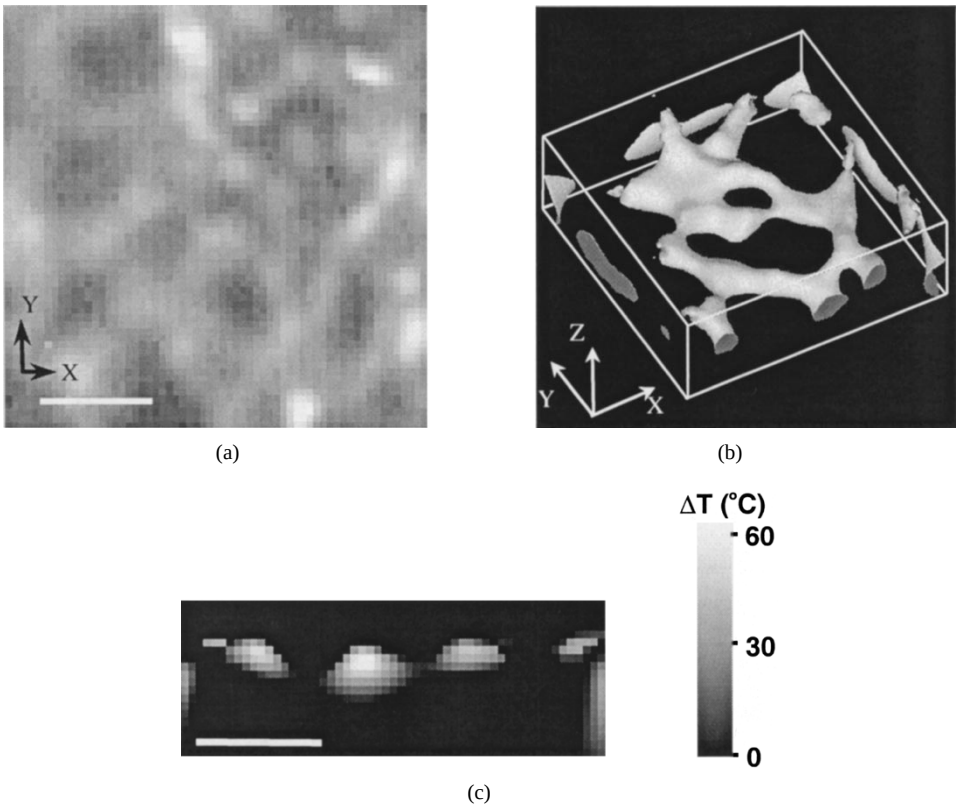

(a) (b) (c)

Fig. 4. (a) Infrared emission image of PWS skin surface recorded immediately after pulsed laser exposure. (b) 3-D view of the initial space-dependent temperature increase in PWS blood vessels (box dimensions $1.65 \times 1.65 \times 0.6$ mm^3) computed by our TRA after 40 iterations (isothermal surface at $\Delta T = 25$ °C). (c) Cross-sectional image (X–Z plane) of the computed initial temperature increase. Scale bar equals 500 μm.

Selected IR images acquired 8 ms apart [Fig. 2(b) and (c)] demonstrate a representative thermal response of the CAM vasculature to pulsed laser exposure (3.4 J/cm^2). Result of the tomographic reconstruction for the region of interest after thirty iterations of the nonnegatively constrained conjugate gradient TRA is shown in Fig. 2(d) as an isothermal surface at $\Delta T(x, y, z, t = 0) = 24$ °C. Vascular features of the CAM observed in the video camera prior to pulsed laser exposure are apparent in the reconstructed image of the initial temperature increase. Inasmuch as delayed IR emission originates from deeper blood vessels, the computed initial temperature increase may be used to assess the depth of vascular components. The video image shown in Fig. 3(a) contains CAM blood vessels in the field of view ranging in diameter between 30–500 μm. The initial temperature increase computed after thirty iterations of the TRA [Fig. 3(b)] and its cross-sectional image at $x = 510$ μm [Fig. 3(c)] show that capillary vessels are confined to a superficial layer 100 μm thick while the temperature increase in the large blood vessel is located approximately 400 μm below the surface. Although the ill-posed nature of the photothermal imaging problem and limitations of the IR instrumentation restrict the imaging depth, results obtained for the CAM vascular model indicate the nonnegatively constrained conjugate gradient TRA may be successfully applied to compute the initial 3-D temperature increase in subsurface blood vessels located within a 600-μm layer.

Although the results are encouraging, application of IR imaging to determine the 3-D laser-induced temperature increase in human skin that contains distributions of two chromophores such as epidermal melanin and hemoglobin, requires additional data analysis. We modified our technique to image individual laser-heated PWS blood vessels. Human subjects for these studies were recruited from the patient population currently receiving PWS laser therapy at the Beckman Laser Institute and Medical Clinic, University of California at Irvine; the experimental protocol was approved by the Institutional Review Board (IRB).

Pulsed radiation ($\lambda = 585$ nm, $t_p = 0.45$ ms) emitted by a flash-lamp pumped pulsed dye laser (Candela, SPTL-1, Wayland, MA) at a dosage of 6 J/cm^2 was used to heat PWS lesions. Typically, the photothermal response of PWS skin to pulsed laser exposure consists of an initial rapid temperature rise due to melanin heating and a slower delayed increase due to heat diffusion from deeper blood vessels to the skin surface [21]. Because the lateral distribution of the initial temperature increase in epidermal melanin immediately following pulsed laser exposure is nearly uniform, energy is concentrated in low spatial frequency components of IR images. In contrast, the initial 3-D temperature increase in hemoglobin is confined to discrete volumes within the lumens of subsurface blood vessels, corresponding spectra contain greater energy in higher spatial frequency components. Immediately after pulsed laser exposure ($\approx$1 ms), heat diffusion is negligible and recorded IR emission images of the skin surface show a complex pattern [Fig. 4(a)] due to the combined heating of epidermal melanin and hemoglobin in PWS blood vessels. The

most superficial blood vessels in the upper dermis heated by absorption of pulsed laser radiation can be observed in the early-time IR images. The wide variation of spatial frequency spectra resulting from heating of melanin and hemoglobin complicates the IR tomographic reconstruction problem. As a first step toward a solution, we developed a simple subtraction procedure to generate a time-sequence of IR emission images $\Delta M_{\mathrm{BV}}(x,y,t)$ exclusively due to PWS blood vessel heating. In this approach, the radiometric temperature increase due to epidermal melanin heating ΔM_{EM} was subtracted from the time sequence of recorded IR emission images $\Delta M(x,y,t)$:

$$\Delta M_{\mathrm{BV}}(x,y,t) = \Delta M(x,y,t) - \Delta M_{\mathrm{EM}}.$$

Magnitude of ΔM_{EM} was determined by identifying pixels absent of blood vessel heating in IR emission images recorded immediately after pulsed laser exposure (dark regions in Fig. 4(a)). The average value of the radiometric temperature increase in the "bloodless" pixels was used to infer ΔM_{EM}. The modified time-sequence of IR emission images was used as input data for our nonnegatively constrained conjugate gradient TRA to compute the initial 3-D temperature increase in PWS blood vessels. A 3-D view of an isothermal surface ($\Delta T = 25$°C) computed by the TRA after 40 iterations [Fig. 4(b)] indicates regions of localized heating due to absorption of pulsed laser radiation in subsurface blood vessels. The computed initial space-dependent temperature increase reveals a network of superficial PWS blood vessels located 150–350 μm below the air–skin interface (Fig. 4(c)). Infrared data show that localized temperature increase may exceed 60 °C in discrete blood vessels. Although, the simple subtraction procedure allows reconstruction of the initial temperature increase in PWS blood vessels, preliminary experiments (not reported here) indicate a more detailed data analysis is required for patients with an extensive distribution of smaller caliber blood vessels in the upper dermis.

V. Conclusion

Our experiments demonstrate the IR imaging technique may be successfully applied to image the laser-induced temperature increase of *in vivo* blood vessels. Use of a high-speed IR-FPA camera in combination with a nonnegatively constrained conjugate gradient TRA provides an experimental means for noncontact tomographic reconstruction of the initial 3-D temperature increase in biological systems. Experiments on the CAM model reveal vascular structure of laser-heated blood vessels within a 600-μm layer. The melanin subtraction procedure introduced for preliminary processing of PWS images, gives IR emission exclusively due to laser-heated blood vessels. The infrared imaging of PWS lesions indicates that localized temperature increase in PWS blood vessels following pulsed laser exposure at 6 J/cm^2 may exceed 60 °C. The tomographic reconstruction of the 3-D temperature increase in PWS immediately following pulsed laser exposure may be useful for assessment of the vascular characteristics of a proposed treatment site and, more importantly, to optimize laser dosimetry required for irreversible destruction of targeted blood vessels throughout an extended treatment protocol.

References

[1] A. C. Tam and B. Sullivan, "Remote sensing applications of pulsed photothermal radiometry," *Appl. Phys. Lett.*, vol. 43, pp. 333–335, 1983.

[2] A. C. Tam, "Pulsed laser photoacoustic and photothermal detection," in *Photoacoustic and Thermal Wave Phenomena in Semiconductors*, A. Mandelis, Ed. New York: North-Holland, 1987, pp. 175–200.

[3] H. Aglan, Z. Zhang, T. Rowell, T. Ahmed, and R. Thomas, "Evaluation of bonded boron/epoxy repairs on aircraft skin," in *Review of Progress in Quantitative Nondestructive Evaluation*, D. O. Thompson and D. E. Chimenti, Eds. New York: Plenum, 1998, pp. 1403–1410.

[4] W. P. Leung and A. C. Tam, "Technique of flash radiometry," *J. Appl. Phys.*, vol. 56, pp. 153–161, 1984.

[5] M. J. C. van Gemert, A. J. Welch, J. W. Pickering, and O. T. Tan, "Laser treatment of port wine stains," in *Optical-Thermal Response of Laser-Irradiated Tissue*, A. J. Welch and M. J. C. van Gemert, Eds. New York: Plenum, 1995, pp. 789–829.

[6] R. E. Fitzpatrick, M. P. Goldman, N. M. Satur, and W. P. Tope, "Pulsed carbon dioxed laser resurfacing of photoaged facial skin," *Arch. Dermatol.*, vol. 132, pp. 395–402, 1996.

[7] B. J. F. Wong, T. E. Milner, H. H. Kim, J. S. Nelson, and E. N. Sobol, "Stress relaxation of porcine septal cartilage during Nd:YAG ($\lambda = 1.32$ μm) laser irradiation: Mechanical, optical and thermal responses," *J. Biomed. Opt.*, vol. 3, pp. 409–414, 1998.

[8] R. R. Anderson and J. A. Parrish, "Microvasculature can be selectively damaged using dye lasers: A basic theory and experimental evidence in human skin," *Lasers Surg. Med.*, vol. 1, pp. 263–276, 1981.

[9] D. Huang, E. A. Swanson, C. P. Li, J. S. Schuman, W. G. Stinson, W. Chang, M. R. Hee, T. Flotte, K. Gregory, C. A. Puliafito, and J. Fujimoto, "Optical coherence tomography," *Science*, vol. 254, pp. 1178–1181, 1991.

[10] A. Yodh and B. Chance, *Spectroscopy and Imaging with Diffusing Light*, *Phys. Today*, vol. 48, pp. 34–40, 1995.

[11] L. Wang, S. L. Jacques, and X. Zhao, "Continuous-wave ultrasonic modulation of scattered laser light to image objects in turbid media," *Opt. Lett.*, vol. 20, pp. 629–631, 1995.

[12] L. T. Norvang, T. E. Milner, J. S. Nelson, M. W. Berns, and L. O. Svaasand, "Skin pigmentation characterized by visible reflectance measurements," *Lasers Med. Sci.*, vol. 12, pp. 99–112, 1997.

[13] C. Xu, J. Guild, W. W. Webb, and W. Denk, "Determination of absolute two-photon excitation cross sections by in situ second-order autocorrelation," *Opt. Lett.*, vol. 23, pp. 2372–2374, 1995.

[14] C. G. A. Hoelen, F. F. M. de Mul, R. Pongers, and A. Dekker, "Three-dimensional photoacoustic imaging of blood vessels in tissue," *Opt. Lett.*, vol. 23, pp. 648–650, 1998.

[15] M. J. C. van Gemert and A. J. Welch, "Approximate solutions for heat conduction: Time constants," in *Optical-Thermal Response of Laser-Irradiated Tissue*, A. J. Welch and M. J. C. van Gemert, Eds. New York: Plenum, 1995, pp. 425–443.

[16] D. M. Goodman, E. M. Johansson, and T. W. Lawrence, "On applying the conjugate-gradient algorithm to image processing problems," in *Multivariate Analysis: Future Directions*, C. R. Rao, Ed. Amsterdam, The Netherlands: North-Holland, 1993, pp. 209–232.

[17] T. E. Milner, D. M. Goodman, B. S. Tanenbaum, and J. S. Nelson, "Depth profiling of laser-heated chromophores in biological tissues by pulsed photothermal radiometry," *J. Opt. Soc. Amer. A*, vol. 12, pp. 1479–1488, 1995.

[18] C. W. Groetsh, *The Theory of Tikhonov Regularization for Fredholm Equations of the First Kind*. Marshfield, MA: Pitman, 1984.

[19] P. C. Hansen and D. P. O'Leary, "The use of L-curve in the regularization of discrete ill-posed problems," *SIAM J. Sci. Comp.*, vol. 14, pp. 1487–1503, 1993.

[20] S. Kimel, L. O. Svaasand, M. Hammer-Wilson, M. J. Schell, T. E. Milner, J. S. Nelson, and M. W. Berns, "Differential vascular response to laser photothermolysis," *J. Invest. Dermatol.*, vol. 103, pp. 693–700, 1994.

[21] S. L. Jacques, J. S. Nelson, W. H. Wright, and T. E. Milner, "Pulsed photothermal radiometry of port-wine-stain lesions," *Appl. Opt.*, vol. 32, pp. 2439–2446, 1993.

Sergey A. Telenkov, for photograph and biography, see this issue, p. 1102.

B. Samuel Tanenbaum (M'75–SM'97), for photograph and biography, see this issue, p. 1066.

Dennis M. Goodman, for photograph and biography, see this issue, p. 1066.

J. Stuart Nelson, for photograph and biography, see this issue, p. 1066.

Thomas E. Milner, for photograph and biography, see this issue, p. 1066.